Autophagy modulates dynamics of connexins at the plasma membrane in a ubiquitin-dependent manner

Eloy Bejarano[a,*], Henrique Girao[b,*], Andrea Yuste[a], Bindi Patel[a], Carla Marques[b], David C. Spray[c], Paulo Pereira[b], and Ana Maria Cuervo[a]

[a]Department of Development and Molecular Biology, Albert Einstein College of Medicine, New York, NY 10461; [b]Center of Ophthalmology and Vision Sciences, Institute for Biomedical Research in Light and Image, Faculty of Medicine, University of Coimbra, Coimbra 3004-548, Portugal; [c]Department of Neurosciences, Albert Einstein College of Medicine, New York, NY 10461

ABSTRACT **Different pathways contribute to the turnover of connexins, the main structural components of gap junctions (GJs). The cellular pool of connexins targeted to each pathway and the functional consequences of degradation through these degradative pathways are unknown. In this work, we focused on the contribution of macroautophagy to connexin degradation. Using pharmacological and genetic blockage of macroautophagy both in vitro and in vivo, we found that the cellular pool targeted by this autophagic system is primarily the one organized into GJs. Interruption of connexins' macroautophagy resulted in their retention at the plasma membrane in the form of functional GJs and subsequent increased GJ-mediated intercellular diffusion. Up-regulation of macroautophagy alone is not sufficient to induce connexin internalization and degradation. To better understand what factors determine the autophagic degradation of GJ connexins, we analyzed the changes undergone by the fraction of plasma membrane connexin 43 targeted for macroautophagy and the sequence of events that trigger this process. We found that Nedd4-mediated ubiquitinylation of the connexin molecule is required to recruit the adaptor protein Eps15 to the GJ and to initiate the autophagy-dependent internalization and degradation of connexin 43. This study reveals a novel regulatory role for macroautophagy in GJ function that is directly dependent on the ubiquitinylation of plasma membrane connexins.**

Monitoring Editor
Tamotsu Yoshimori
Osaka University

Received: Oct 11, 2011
Revised: Mar 26, 2012
Accepted: Apr 5, 2012

INTRODUCTION

Intercellular communication is essential in pluricellular organisms to facilitate the flow of information among neighboring cells. Metabolic and electric cellular coupling are achieved through gap junctions (GJs), a highly conserved communication system that allows for the diffusion of molecules smaller than 1 kDa (Kumar and Gilula, 1996). GJs are exceptionally differentiated domains in the plasma membrane containing multiple-span membrane proteins called connexins. In contrast to other membrane proteins, all members of the connexin (Cx) family display remarkably short half-lives. Regulated turnover of Cx is crucial for maintaining the activity and stability of GJs. In fact, altered degradation of Cx has been shown to underlie the basis of different pathologies (VanSlyke *et al.*, 2000; Berthoud *et al.*, 2003). Both the ubiquitin–proteasome system and lysosomes have been described as participating in degradation of GJ plaques and their individual components. We previously showed that ubiquitinylation of Cx43 incorporated into hemichannels triggers internalization and degradation of GJs by a mechanism that requires the endocytic adaptor Eps15 (Girao *et al.*, 2009; Catarino *et al.*, 2011). The present work focuses on the contribution of autophagy to the regulation of three well-characterized Cx—namely

This article was published online ahead of print in MBoC in Press (http://www.molbiolcell.org/cgi/doi/10.1091/mbc.E11-10-0844) on April 11, 2012.

*These authors contributed equally to this work.

Address correspondence to: Paulo Pereira (ppereira@ibili.uc.pt), Ana Maria Cuervo (ana-maria.cuervo@einstein.yu.edu).

Abbreviations used: 3MA, 3 methyladenine; Cx, connexin; Eps15, epidermal growth factor receptor; GFP, green fluorescent protein; GJ, gap junctions; LC3, light chain 3 protein; MEFs, mouse embryonic fibroblasts; Nedd4, neuronal precursor cell–expressed developmentally downregulated 4; RFP, red fluorescent protein.

Cx43, 26, and 32—and on the role of ubiquitin in this regulation, by using Cx43 as a model.

Among the mechanisms for the degradation of intracellular components in lysosomes or autophagy, the most quantitatively important form is macroautophagy, which involves the formation of a double-membrane vesicle (autophagosome) through the elongation of a de novo formed membrane that seals on itself, sequestering cargo inside. This double-membrane vesicle fuses with lysosomes, thus acquiring proteolytic enzymes to form a mixed compartment, or autophagolysosome, where the cargo is ultimately degraded. The participation of lysosomes in the degradation of GJ channels was proposed >30 years ago based on elegant ultrastructural studies. For a long time, however, this connection with lysosomes was proposed to occur solely through endocytic delivery of plasma membrane regions to lysosomes (Ginzberg and Gilula, 1979; Pfeifer, 1980). On the basis of biochemical and structural approaches, recent studies now support the involvement of autophagy in connexin degradation (Hesketh *et al.*, 2010; Lichtenstein *et al.*, 2011). However, the reasons for the redundancy of proteolytic systems in connexin turnover, the pool of connexin (intracellular or GJ) targeted for degradation through each pathway, the molecular markers that trigger delivery of Cx to autophagosomes, and the consequences of changes in autophagy on Cx function are for the most part unknown.

In this study, we characterized the involvement of macroautophagy in the turnover of GJs by analyzing in vitro and in vivo the effects of changes in the activity of this pathway on the levels, cellular distribution, and function of three different Cxs. We provide evidence for a novel role of macroautophagy on the regulation of plasma membrane levels of Cxs and consequently in modulating the communication among adjacent cells. Furthermore, our studies dissect the early events that trigger GJs for macroautophagic degradation and reveal a previously unknown interplay between the ubiquitin system and autophagy in the regulation of functional GJs.

RESULTS

Connexins associate with autophagic compartments in a nutrient-regulated manner

Recent studies revealed the contribution of macroautophagy to Cx degradation (Hesketh *et al.*, 2010; Lichtenstein *et al.*, 2011). However, the origin of the degraded Cx—intracellular compartments or GJs at the plasma membrane—and whether or not autophagic degradation affects GJ functionality remain unclear. To gain further insights into Cx autophagy, we first confirmed the presence of different Cxs in autophagic vacuoles in the two experimental systems used in this study, rodent liver and different cell types in culture. Immunoblot of mouse liver subcellular fractions for three of the Cxs expressed in this tissue—Cx43, Cx32, and Cx26—revealed the presence of these three proteins in secondary lysosomes and at higher levels in autophagosomes and autophagolysosomes (Figure 1A; total levels in homogenate and enrichment of autophagic/lysosomal markers in this fractions are shown in Figure 1E and Supplemental Figure S1A). Immunofluorescence analysis of these same fractions isolated from mice expressing green fluorescent protein (GFP) fused to LC3 (a well-established autophagosome marker; Kabeya *et al.*, 2000) confirmed that Cx indeed colocalized with GFP-LC3–positive vesicles, thus discarding possible contamination of other Cx-containing structures in this preparation (Supplemental Figure S1B). Immunogold staining of isolated lysosomes and autophagosomes for the different Cxs (Figure 1B and Supplemental Figure S1C) and immunofluorescence confocal microscopy for LC3 and Cxs in cultured cells (Figure 1C) also confirmed the presence of the three Cxs in vesicles from the autophagic system.

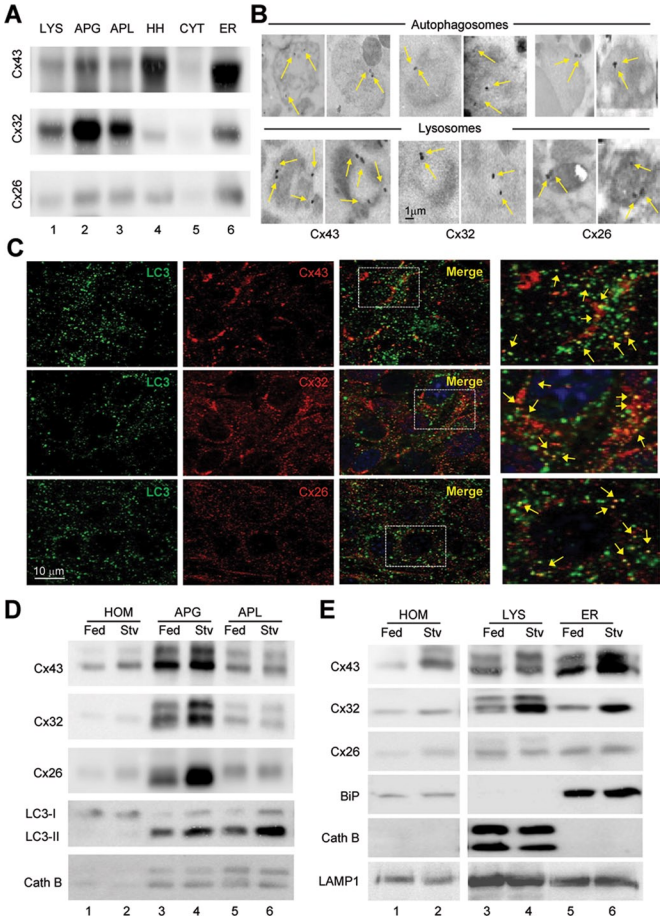

FIGURE 1: Association of connexins with compartments of the autophagic/lysosomal system is modulated by starvation. (A) Immunoblot for the indicated Cx of subcellular fractions (100 μg of protein/lane) isolated from 6-h-starved mice liver. APG, autophagosomes; APL, autophagolysosomes; CYT, cytosol; ER, endoplasmic reticulum; HH, heart homogenate run as positive control for Cx43; LYS, lysosomes; Homogenates are shown in E. (B) Immunogold for the indicated Cxs in lysosomes and autophagosomes isolated from fed mouse liver (complete field images are shown in Supplemental Figure S1C). (C) Immunofluorescence for LC3 and the indicated Cxs in MEF cells. Individual channels, merge, and colocalization regions are shown. Right, a higher-magnification inset; arrows indicate colocalization. (D, E) Immunoblots for the indicated Cxs of autophagic vacuoles (D; APG, autophagosomes; APL, autophagolysosomes) and lysosomes (E; 50 μg of protein/lane) isolated from livers of fed or 6-h-starved (Stv) mice. Controls for purity in each fraction include ER marker (BiP), lysosomal hydrolase (cathepsin B), autophagosomal marker (LC3), and LAMP1.

We then determined the effect of up-regulating macroautophagic activity on the levels of Cxs associated with the autophagic compartments. We used starvation, one of the best-characterized physiological stimuli for triggering macroautophagy. Immunoblot for the three Cxs in autophagosomes and lysosomes isolated from starved mouse livers revealed higher enrichment for the three proteins in these compartments upon starvation (Figure 1, D and E, and Supplemental Figure S1D). In fact, we found about a twofold increase in the amount of total cellular Cx recovered in these compartments when isolated from animals starved for 6 h (Supplemental Figure S1D). Similar increase in the abundance of Cxs in autophagic compartments could be reproduced in cultured cells upon serum

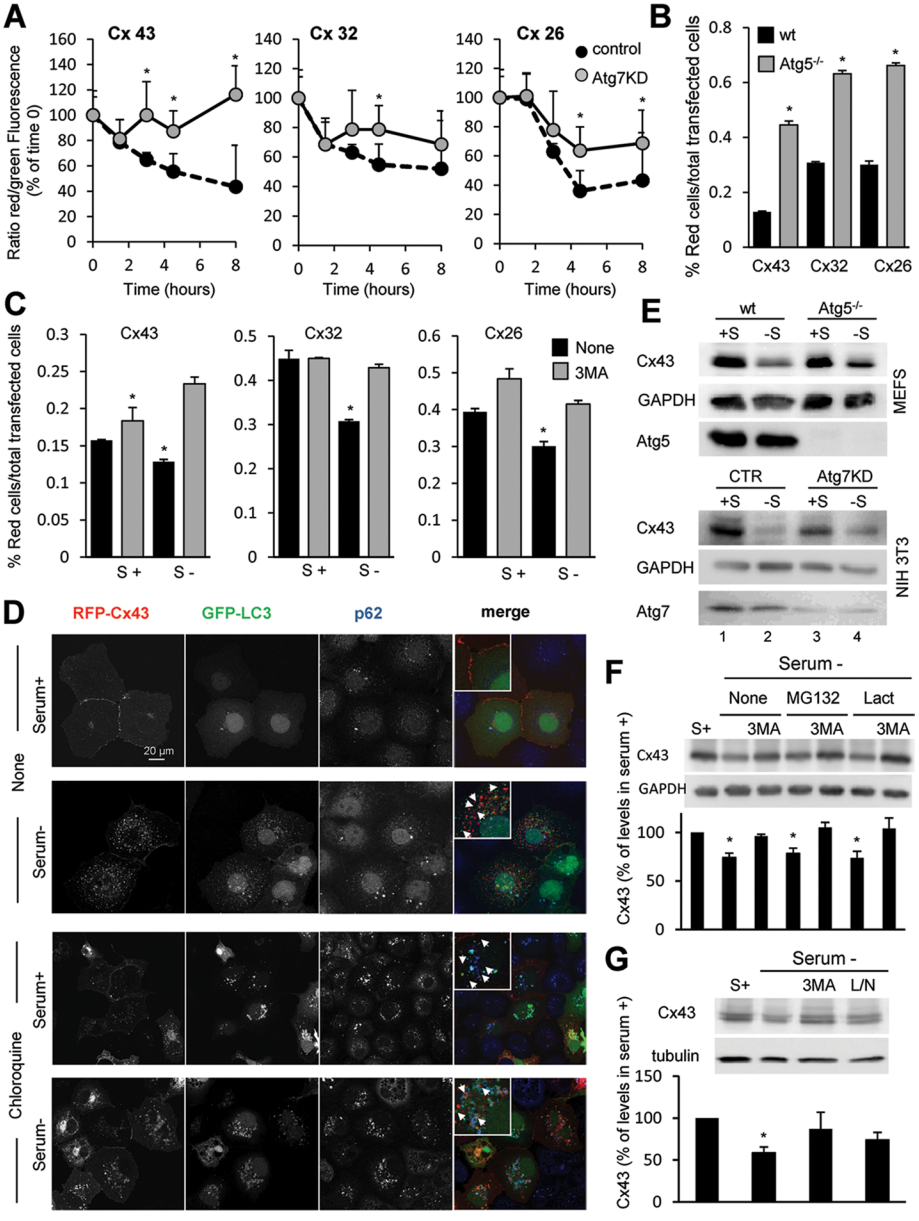

FIGURE 2: Degradation of connexins is compromised by blockage of macroautophagy. (A) Kinetics of fluorescence decay in wild-type and Atg7-knockdown NIH3T3 cells transfected with a vector expressing Dendra fused to the indicated Cx imaged at different times after photoactivation. The ratio of red to green fluorescence was calculated at each time point. Values are expressed as percentage of the ratio at time 0 and are mean ± SEM (n = 3). (B, C) MEFs from wild-type and Atg5-null mice (Atg5$^{-/-}$; B) or NIH3T3 fibroblasts (C) transfected with the same constructs as in A were incubated after photoactivation in the presence or absence of serum and 3MA as labeled. Quantification of red fluorescence decay by FACS analysis calculated as the percentage of total red fluorescence in each sample normalized against the total number of cells expressing Dendra-Cx. Values are mean ± SEM (n = 3). Significant differences with wild-type cells are indicated. (See representative scatterdot plot for each different condition in Supplemental Figure S2.) (D) COS-7 cells transfected with RFP-Cx43 and GFP-LC3 were maintained in the presence or absence of serum and treated or not with chloroquine as labeled. Immunofluorescence for p62 (blue) and the fluorescence in the red (Cx43) and green (LC3) channels is shown. Right, a merged image; inset shows detail at higher magnification. (E) Immunoblot for Cx43 and the indicated Atg in MEFs from wild-type or Atg5-null mice or in NIH3T3 fibroblasts control or knocked down for Atg7 maintained in the presence or absence of serum for 8 h. (F, G) Immunoblots for Cx43 of NIH3T3 cells incubated in the presence (S+) or absence of serum and treated for 8 h with two different proteasome inhibitors (MG132 or lactacystin [Lact]), 3MA, and a combination of leupeptin and ammonium chloride (L/N). Top, representative immunoblots. Bottom, changes in Cx43 levels calculated by densitometric quantification of blots like the ones shown here.

removal (Supplemental Figure S2; note the increased colocalization with LC3-positive compartments and further increase in colocalization when degradation in the lysosomal compartment was prevented by chloroquine).

In summary, in agreement with previous reports (Lichtenstein *et al.*, 2011), we demonstrate, using biochemical and image-based procedures, the association of Cxs to autophagic compartments and an increase in the delivery of Cxs to autophagic vacuoles upon macroautophagy activation.

Inhibition of macroautophagy slows down degradation of connexins

We next analyzed the effect that blocking macroautophagy had on the degradation of Cxs in cultured cells. To this purpose, we transfected wild-type cells and cells with compromised macroautophagy (knocked down for the essential autophagy gene *ATG7*) with vectors coding for the photoswitchable fluorescent protein Dendra in-frame with the full-length sequence of each of the Cxs of interest. Photoconversion of Dendra from green to red fluorescence allows for tracking the kinetics of degradation of the pool of photoconverted protein without the need to block protein synthesis, as the de novo synthesized protein will fluoresce in green (Supplemental Figure S3A). As shown in Figure 2A, we found similar kinetics for the degradation of the three Dendra-Cxs upon serum removal in wild-type cells, and, in all cases their degradation was compromised in Atg7-knockdown cells, supporting the contribution of macroautophagy to their normal turnover. Of interest, the effect of macroautophagy blockage was more pronounced in the degradation of Cx43 when compared with Cx32 or Cx26 (Figure 2A), which points to a differential contribution of macroautophagy to the degradation of different Cxs. Similar results were observed after FACS analysis (Figure 2B and S3B, C). In this case, cells were scored as positive for red fluorescence after thresholding for detected fluorescence in untransfected cells or cells transfected but not photoconverted (Supplemental Figure S3A). Fluorescence-activated cell sorting (FACS) analysis of photoconverted mouse embryonic fibroblasts (MEFs) from mice null for

Values are expressed as percentage of Cx43 present in cells maintained in serum-supplemented media and are mean ± SEM (n = 3). *p < 0.05. Significant differences with respect to control, wild type, or serum+.

ATG5, another essential autophagy gene, confirmed that complete genetic blockage of macroautophagy also resulted in severe compromise of the serum-induced degradation of all three Cxs (Figure 2B and Supplemental Figure S3, B and C; 69% blockage in degradation of Cx43 compared with 48 and 50% for Cx32 and Cx26, respectively). As in the other cell types, Cx43 degradation was faster than that of Cx32 and Cx26 in MEFs, and genetic blockage of macroautophagy had a more prominent effect on Cx43 kinetics even in serum-supplemented cells (Supplemental Figure S3B; 66% blockage in degradation of Cx43 compared with 20 and 26% for Cx32 and Cx26, respectively).

To further validate the contribution of macroautophagy to Cx degradation, we examined the effect of acutely blocking this catabolic pathway by pharmacological treatment with the PI3K inhibitor 3-methyladenine (3MA), which is well established to inhibit autophagosome formation (Seglen and Gordon, 1982). We found slowdown in the decay of red fluorescence induced by serum removal in the cells treated with 3MA for all three Cxs (Figure 2C and Supplemental Figure S3B). This effect was less evident when cells were maintained in the presence of serum during the whole experiment (Supplemental Figure S3B), which supports a predominant role of macroautophagy in the degradation of Cxs in response to nutritional stress. As with the genetic manipulations, Cx43 degradation was more severely affected by the treatment with 3MA than were the other Cxs (Figure 2C and Supplemental Figure S3B; 48% blockage in degradation of Cx43 compared with 28 and 25% for Cx32 and Cx26, respectively). MEFs from mice null for *ATG5* displayed loss of their sensitivity to 3MA, confirming that the effect of the inhibitor was due to its ability to block macroautophagy (Supplemental Figure S3, B and C).

Fluorescence analysis of cells expressing a red fluorescent protein (RFP) fused in the N-terminus of Cx43 (RFP-Cx43) revealed that, upon serum removal, Cx43 relocalized from the plasma membrane to intracellular vesicles positive for LC3 and p62, a structural component and a common cargo protein in autophagosomes, respectively (Figure 2D). Blockage of lysosomal degradation by treatment with the pH-neutralizing agent chloroquine enhanced the content of Cx43 in the LC3/p62–positive compartments, supporting its degradation by macroautophagy (Figure 2D).

Although the recombinant proteins were expressed at very low levels to avoid accelerated degradation due to overexpression, to eliminate the possibility that the changes in degradation were intrinsic to the exogenously expressed protein, we then compared the effect of manipulations in macroautophagic activity on the intracellular levels of endogenous Cx43. This is the most ubiquitously expressed Cx and, in addition, of the three Cxs analyzed it seemed the most dependent on macroautophagy for its degradation. Removal of serum for 8 h was enough to reduce the endogenous intracellular levels of Cx43 by 50% in MEFs and by 78% in NIH3T3 cells (Figure 2E). This starvation-induced decrease in Cx43 levels was not eliminated, but it was reduced 30–45% in Atg5-knockout MEFs or after Atg7 knockdown in NIH3T3 (Figure 2E).

Because the ubiquitin–proteasome system is involved in the basal degradation of different Cxs (Leithe *et al.*, 2009), we then analyzed the contribution of the two main proteolytic systems to the degradation of Cx43 in response to nutrient deprivation. Treatment of cells with two widely used proteasomal inhibitors (MG132 or lactacystin) did not result in significant decrease in the starvation-induced degradation of Cx43, nor did they have an additive effect when administered together with 3MA (Figure 2F). In contrast, blockage of lysosomal proteolysis by a combination of ammonium chloride and leupeptin had a similar effect to that observed with 3MA, supporting once again that the effect of this kinase inhibitor was at the level of macroautophagy (Figure 2G). Taken together, our results support that macroautophagy is primarily responsible for the starvation-induced degradation of Cxs and in particular of Cx43.

Connexin43 localized at the plasma membrane is the main target of macroautophagy-dependent degradation

Previous studies described that monomers or oligomers of Cxs can be directly targeted to lysosomes from early secretory compartments and that Cxs at the plasma membrane (hemichannels or GJs) can also end up in lysosomes after internalization via endocytosis (VanSlyke *et al.*, 2000; Qin *et al.*, 2003).

To elucidate the pool of cellular Cx43 subjected to the macroautophagic process described in the previous sections, we first performed biotinylation assays to evaluate the levels of Cx43 localized at the plasma membrane. As shown in Figure 3A, removal of serum induced a marked decrease in the amount of Cx43 localized at the cell surface. Consistently, inhibition of macroautophagy by 3MA resulted in a marked increase of Cx43 at the plasma membrane, both under control conditions and especially in response to starvation. To further evaluate the effect of starvation on Cx43 localized specifically at the GJ plaques, we separated Cx43 into Triton X-100–soluble and Triton X-100–insoluble fractions, which were shown previously to be enriched in non–gap junctional and gap junctional Cx43, respectively (VanSlyke *et al.*, 2000; Govindarajan *et al.*, 2010; Catarino *et al.*, 2011). Comparison of the kinetics of degradation of Cx43 in both fractions upon blockage of protein synthesis with cycloheximide revealed that removal of serum particularly accelerated degradation of Cx43 localized at GJs (Figure 3, B and C). Indeed, whereas the stability of the Triton-soluble Cx43 was not significantly altered by starvation, the half-life of Cx43 localized at GJs decreased from more than 6 h to 3 h upon serum removal (Figure 3C). Addition of the inhibitor of lysosomal proteolysis (chloroquine or ammonium chloride/leupeptin) and of 3MA to inhibit macroautophagy revealed that most Cx43 localized at GJs was degraded by macroautophagy upon serum removal, whereas macroautophagy contributed to only 20% of the degradation of this protein under normal conditions (Figure 3D). Chloroquine had a very discrete stabilizing effect on detergent-soluble Cx43, and the effect of 3MA on this fraction of Cx43 was negligible both in the presence or absence of serum (Figure 3D). Taken together, the foregoing results support that it is Cx43 that is present at plasma membrane and, in particular, at GJs that is targeted for degradation by macroautophagy.

To further confirm the preferential macroautophagy of Cx43 at the plasma membrane, we used confocal microscopy to analyze the effect of pharmacological and/or genetic blockade of macroautophagy on intracellular and plasma membrane levels of Cx43. As shown in Figure 3E, addition of 3MA prevented the disappearance of Cx43 from the plasma membrane induced by serum deprivation in cells expressing GFP-Cx43. This treatment was also effective in blocking the marked decrease in endogenous Cx43 immunoreactivity at the plasma membrane observed in wild-type NIH3T3 cells upon serum removal (Figure 3F; note that we used reverse contrast images here to better contrast Cx43 located at the plasma membrane against the higher intracellular content of Cx43 observed in NIH3T3 cells). Consistent with these findings, we observed a marked increase in the number of Cx43-positive fluorescent puncta in cells knocked down for Atg7, and removal of serum in the presence or absence of 3MA did not have a significant effect on Cx43 content in these cells (Figure 3, F and G). Similar results were observed in MEFs from Atg5-null mice, with a marked increase in the immunoreactivity at the plasma membrane of these cells even under basal conditions,

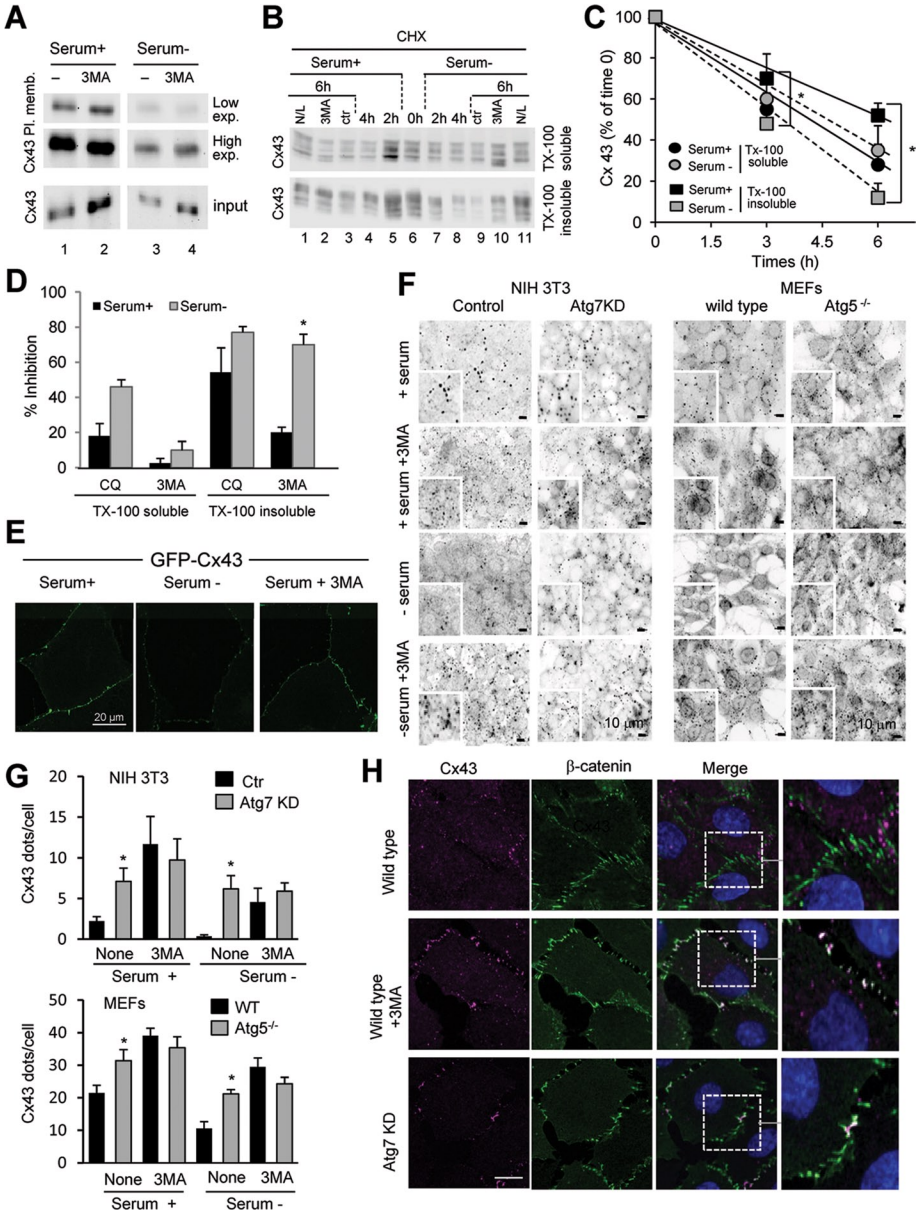

FIGURE 3: Macroautophagy degrades preferentially Cx43 in GJs at the plasma membrane. (A) COS-7 cells transfected with Cx43 were maintained in the presence or absence of serum and treated or not with 10 mM 3MA as labeled. Cells were then subjected to cell surface protein biotinylation, and the biotinylated fraction of the cell lysates was precipitated with NeutrAvidin beads. Precipitates were then analyzed by Western blot using polyclonal antibodies against Cx43. (B) COS-7 cells transfected with Cx43 were treated with cycloheximide (CHX) for the indicated times either in the presence or absence of serum. Lysates were subjected to extraction with 1% Triton X-100, and soluble and insoluble fractions were processed for immunoblot against Cx43. Where indicated 10 mM 3MA or 20 mM ammonium chloride and 100 µM leupeptin (N/L) was added to the incubation media during the chase. (C) The kinetics of degradation of Cx43 in each condition was calculated by densitometry of immunoblots like the one shown and plotted in a graph. (D) Inhibitory effect of CQ and 3MA in the degradation of Cx43 in each fraction calculated by densitometric quantification of blots like the ones in A. Values are expressed as percentage of inhibition and are mean ± SEM (n = 3). (E) Confocal microscopy of cells expressing GFP-Cx43 maintained in the presence or absence of serum and supplemented with 3MA as indicated. (F) Immunofluorescence (inverted grayscale images) of Cx43 in NIH3T3 cells control or knocked down for Atg7 (left) and in MEFs from wild-type or Atg5-null mice (right) maintained for 8 h in serum-supplemented or serum-deprived media in presence or not of 3MA as indicated. (G) Quantification of number of Cx43-positive fluorescent puncta per cell. Values are mean ± SEM (n = 3; >45 cells counted per experiment). (H) Immunofluorescence for Cx43 and β-catenin in NRK cells control, knocked down for Atg7, or exposed to 10 mM 3MA for 8 h. Individual channels and merged channel images are shown. Right, higher-magnification of insets. *p < 0.05. Significant differences with respect to control or serum+.

which remained unchanged upon serum removal or treatment with 3MA (Figure 3, F and G). Costaining for Cx43 and the bona fide membrane marker β-catenin confirmed that Cx43 was indeed retained at the plasma membrane upon treatment with 3MA or knockdown for Atg7 (Figure 3H shows costaining in normal rat kidney [NRK] cells). Overall, our data suggest that changes in macroautophagic activity have a marked effect on the levels of Cx43 in GJs.

Macroautophagic blockage increases gap junction intercellular communication

To determine whether the changes observed in the intracellular levels and distribution of Cx43 upon blockage of macroautophagy also occurs in vivo when considering a whole organ, we crossed ATG7$^{f/f}$ mice with mice expressing Cre recombinase under the control of the albumin promoter to generate mice with compromised macroautophagy in the liver (Alb-Cre-ATG7$^{f/f}$; Atg7$^{-/-}$). Immunoblot in livers of these animals revealed a marked increase in total levels of Cx43 in the knockout mice (approximately fivefold) when compared with wild-type littermates (Figure 4A). Immunohistochemical analysis of the Alb-Cre-ATG7$^{f/f}$ livers confirmed the higher content of Cx43 in the livers of these mice (Figure 4B). Whereas in wild-type mice Cx43 was mainly diffuse in the cytosol and to a lesser extent in the plasma membrane, livers of Alb-Cre-ATG7$^{f/f}$ mice showed intense Cx43 signal preferentially at the plasma membrane (Figure 4B). These data support the notion that compromise of macroautophagy in vivo results in remarkable qualitative and quantitative changes in hepatic GJs, which could have a marked effect on the intercellular communication in this tissue.

To further explore whether the increase in Cx43 at the plasma membrane observed both in vitro and in vivo upon blockage of macroautophagy had a functional impact on intercellular communication or whether it just represented nonfunctional Cx43 that accumulated in this compartment, we compared GJ permeability between control cells and cells with compromised macroautophagy. We used the standard scrape-loading assay that allows visualization of the diffusion of a low–molecular weight dye permeable through Cx channels. Quantification of the distance from the scrape line reached by the fluorescent dye provides a good assessment of Cx-mediated intercellular communication (el-Fouly *et al.*, 1987). Chemical blockage of macroautophagy with 3MA in NIH3T3 cells increased dye

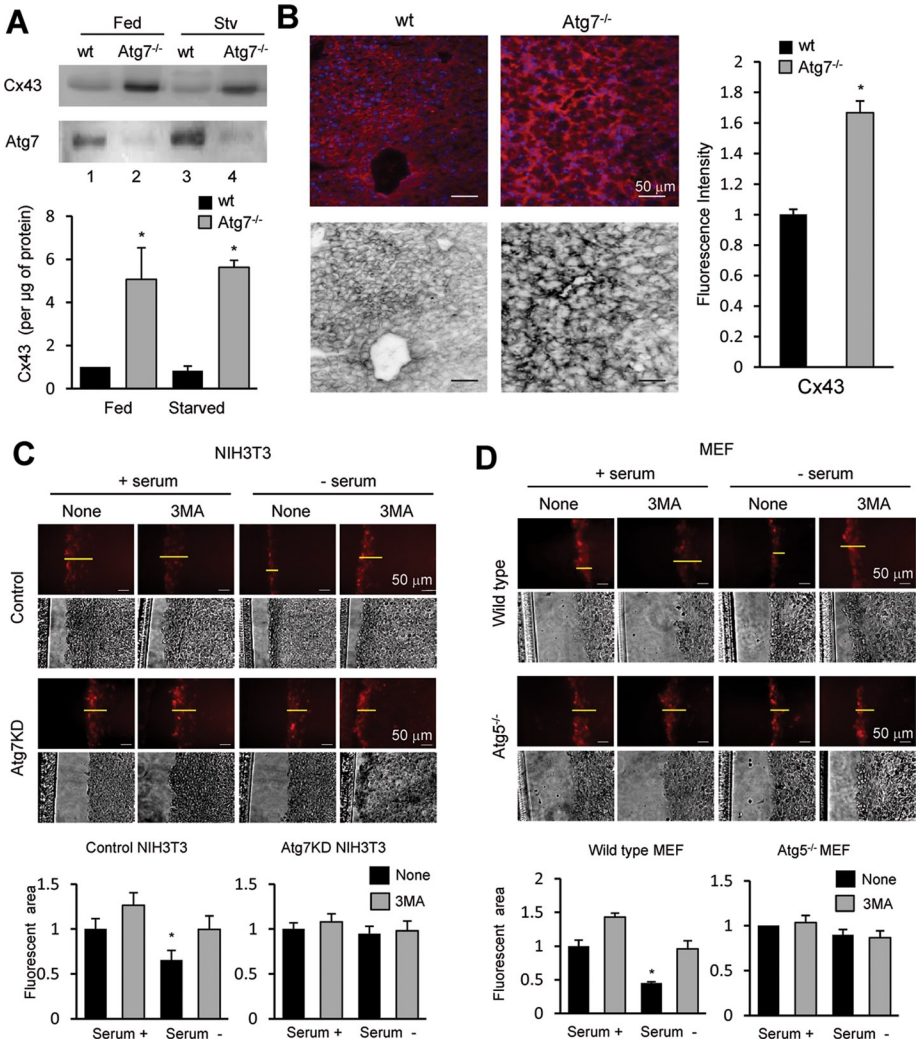

FIGURE 4: Blockage of macroautophagy increases the content of functional GJs. (A) Immunoblot for the indicated proteins of homogenates (50 µg of protein/lane) from livers of fed or 6-h-starved wild-type and Alb-Cre-ATG7$^{f/f}$ mice. Bottom, quantification of enrichment of Cx43 calculated by densitometry of blots like the ones shown here. Values are mean ± SEM (n = 3–5). Significant differences with wild type are indicated. (B) Immunostaining for Cx43 of frozen liver sections from the same mice. Bottom, inverted grayscale images to better visualize GJs. Right, Quantification of changes in fluorescence intensity for Cx43 in the liver sections expressed as fold the intensity in wild type. Values are mean ± SEM (n = 3). (C, D) Scrape loading assay with sulforhodamine B in NIH3T3 cells control or knocked down for Atg7 (C) and MEFs from wild-type mice or mice null for Atg5 (D) incubated in the presence or absence of serum and 10 mM 3MA for 8 h. Histograms at the bottom show the fluorescent area in each condition quantified using Scion Image software relative to the area in control conditions. Values are mean ± SEM (n = 3, with 45 cells counted). *p < 0.05. Significant differences with respect to control.

migration when compared with untreated cells both under basal conditions and, more pronouncedly, upon serum removal (Figure 4C; 48% decrease of migration upon serum removal in untreated cells vs. 12% decrease in migration in 3MA-treated cells). Treatment with 3MA did not affect dye migration in cells knocked down for Atg7, confirming that the drug was acting through blockage of macroautophagy (Figure 4C). In fact, removal of serum in Atg7-knockdown cells did not associate with the reduction of dye migration observed in the control cells. We obtained similar results in MEFs from Atg5-null mice, in which dye migration remained unchanged upon treatment with 3MA or serum removal, in clear contrast to the 60% decrease observed in the wild-type cells (Figure 4D). These results support that the GJs remaining at the plasma membrane upon macroautophagic compromise are functional and reveal a regulatory role for macroautophagy in intercellular communication. This function seems to be particularly noticeable upon nutritional stress, supporting the idea that macroautophagy may be required to diminish gap junction communication when nutrients are scarce.

Blockage of macroautophagy prevents internalization of plasma membrane connexin43

The increase in Cx43 content at the plasma membrane upon blockage of macroautophagy observed both in cultured cells and in vivo could be due to either enhanced affluence of intracellular Cx43 toward the plasma membrane or reduced Cx43 internalization. To distinguish between these two possibilities, we examined the effect of known inducers of Cx43 internalization in macroautophagy-impaired cells. Exposure of wild-type MEFs to lindane (γ-hexachlorocyclohexane), which is known to induce plasma membrane Cx43 internalization and degradation (Guan and Ruch, 1996; Defamie *et al.*, 2001), reduced total cellular levels of Cx43 to 50% after 12 h of treatment under basal conditions (Figure 5A). This effect was completely blocked when 3MA was added to the culture media (Figure 5A). In fact, immunofluorescence analysis confirmed a time-dependent redistribution of most of the cellular Cx43 from the plasma membrane to perinuclear vesicular structures at early times after treatment with lindane followed by its intracellular degradation (Figure 5B and Supplemental Figure S4A). These vesicles were negative for Golgi or early endosome markers but were highlighted with the late endosomal/lysosomal marker lysosome-associated membrane protein type 1 (LAMP-1), supporting their later degradation in this compartment (Supplemental Figure S4B). The Cx43-positive vesicles were no longer evident upon 3MA treatment (Supplemental Figure S4A) or upon genetic blockage of macroautophagy (MEFs from Atg5-null mice; Figure 5B and Supplemental Figure S4A), conditions in which most Cx43 remained at the plasma membrane.

To further demonstrate the interdependence between Cx43 internalization and macroautophagy, we transfected COS-7 cells with an endocytic-impaired form of Cx43 (Cx43Y286A) mutated in the tyrosine sorting signal (Thomas *et al.*, 2003; Catarino *et al.*, 2011). In contrast to the marked decrease of wild-type Cx43 in response to serum removal, the endocytic mutant Cx43 was resistant to macroautophagy-dependent degradation under these conditions (Figure 5C). The accumulation of slower-migrating bands in the mutant Cx43Y286A, corresponding to previously described hyperphosphorylated forms of the protein (Leithe and Rivedal, 2004), suggests

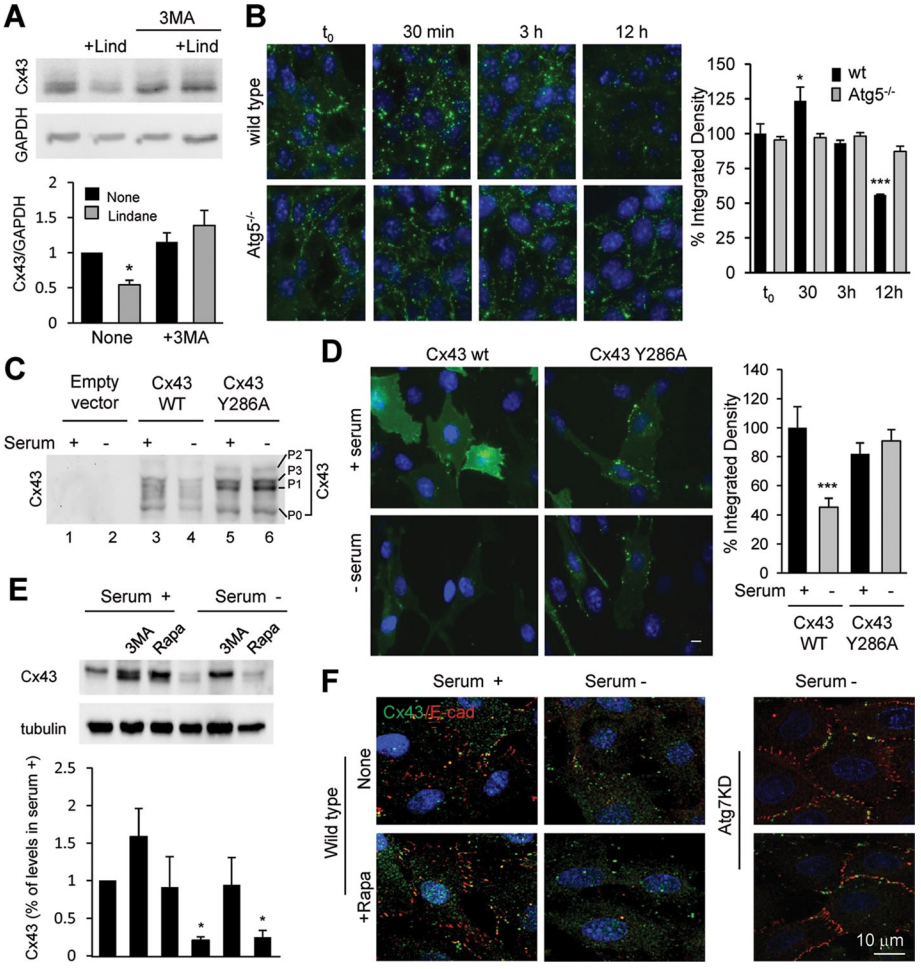

FIGURE 5: Blockage of macroautophagy prevents internalization and degradation of Cx43. (A) Immunoblot (100 μg of protein/lane) for Cx43 in MEFs treated with 100 μM lindane (Lind) for 12 h in presence or absence of 10 mM 3MA. Top, representative immunoblot. Bottom, quantification of total levels of Cx43 relative to values in untreated cells. Values are mean ± SEM (n = 5). Significant differences with respect to untreated cells are indicated. (B) Immunofluorescence for Cx43 in MEFs from wild-type and Atg5-null mice at the indicated times after treatment with lindane. Right, quantification of the decay of signal for Cx43 in both cell types. Values are mean ± SEM (n = 3). Significant differences with respect to untreated cells are indicated. (C) Immunoblot for Cx43 of COS-7 cells transfected with Cx43 wild type (wt) or mutated at tyrosine 286 (Cx43Y286A) and maintained in the presence or absence of serum as indicated. (D) Immunofluorescence for Cx43 of COS-7 transfected with plasmids coding for wt and endocytic mutant (Y286A) Cx43 and maintained in the presence or absence of serum as labeled. Left, representative images. Right, quantification of the integrated density of the signal for Cx43 in both cell types. Values are mean ± SEM (n = 3). Significant differences with respect to cells maintained in serum supplemented media are indicated. (E) NIH3T3 cells incubated in the presence or absence of serum and treated for 8 h with 3MA or rapamycin (Rapa). Top, representative immunoblot. Bottom, changes in Cx43 levels calculated by densitometric quantification of blots like the one shown here. Values are expressed as percentage of Cx43 present in untreated cells maintained in serum-supplemented media and are mean ± SEM (n = 3). Significant differences with respect to untreated serum+ are indicated. (F) Immunofluorescence for Cx43 and E-cadherin in cells maintained in the presence or absence of serum and treated or not with rapamycin (Rapa). Merged channels are shown. Right, similar staining in cells knocked down for Atg7. *p < 0.05. Significant differences with respect to control.

its accumulation at the plasma membrane, as the immunofluorescence analysis also confirmed (Figure 5D). We found that the exogenous GFP-tagged wild-type Cx43 displayed behavior similar to that observed for the endogenous Cx43, in which serum removal induced its internalization and rapid degradation. In clear contrast, GFP-Cx43Y286A remained at GJs in the plasma membrane (Figure 5D). These results support the idea that the recruitment of Cx43 for degradation by macroautophagy requires the prior internalization of the protein. In fact, we found that although blockage of macroautophagy results in retention of Cx43 at the plasma membrane, up-regulation of macroautophagy per se under basal conditions in different cell types such as fibroblasts and hepatocytes is not enough to trigger internalization/degradation of Cx43. Thus treatment of these cells with rapamycin, a well-characterized activator of macroautophagy, by blocking the inhibitory effect of mTOR on this pathway, did not reduce intracellular levels of Cx43 in basal conditions nor did it enhance the degradation of this Cx upon serum removal (Figure 5E). Similarly, levels of Cx43 at the plasma membrane remained unchanged upon rapamycin treatment both in wild-type and in Atg7$^-$knockdown cells (Figure 5F), suggesting that events upstream of macroautophagic activation are required to regulate the internalization/degradation of Cx43 by this pathway.

Macroautophagy of GJ connexin43 requires Nedd4-mediated ubiquitinylation

Posttranslational modifications such as ubiquitinylation and phosphorylation have been shown to modulate the internalization of GJs by endocytosis (Laing and Beyer, 1995; Berthoud *et al.*, 2004; Leithe *et al.*, 2009). To elucidate the mechanisms that trigger macroautophagy-dependent internalization of Cx43 from the plasma membrane, we first compared the isoelectric profile of Cx43 by bidimensional gel electrophoresis in cells maintained in the presence or absence of serum under basal conditions, Cx43 isoforms distribute as an acidic subpopulation preferentially in the 43-kDa region of the gel and a weakly basic subgroup of isoforms with very high molecular weight (Supplemental Figure S5). On serum deprivation, added to the expected decrease in total Cx43 signal we observed a marked decrease in the molecular weight of the basic form of Cx43 toward the 43-kDa region (Supplemental Figure S5).

The higher–molecular weight variants of Cx43 could result, among others, from hyperphosphorylation or ubiquitinylation. Because phosphorylation would shift the isoelectric point toward more acidic variants, we focused on the analysis of polyubiquitinylation as a possible trigger of macroautophagy-mediated Cx43 internalization. We previously showed that the ubiquitin ligase Nedd4 mediates the ubiquitinylation of Cx43 and that the incorporation of ubiquitinylated Cx43 in hemichannels induces the internalization and degradation of GJs by recruiting the endocytic protein epidermal growth factor

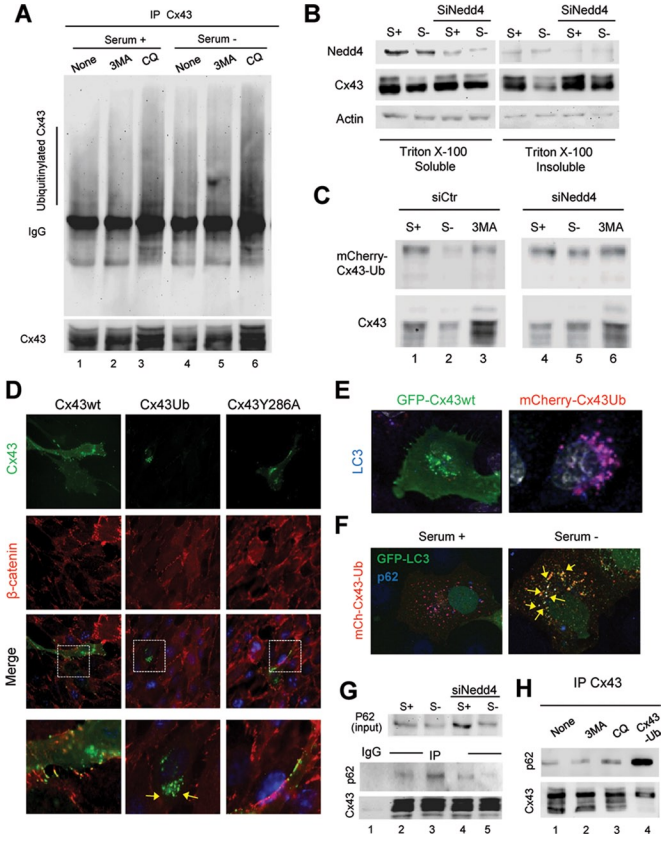

FIGURE 6: Macroautophagy of Cx43 in GJs requires its prior ubiquitinylation. (A) COS-7 cells expressing Cx43 untreated (none) or treated with 10 mM 3-methyladenine or 10 mM chloroquine and maintained in the presence or absence of serum were subjected to immunoprecipitation for Cx43 and immunoblotted for Cx43 or ubiquitin (exposure time on the right has been selected to equal the intensity of the Cx43 bands and enable better appreciation of the differences in intensity of ubiquitinylation). (B) COS-7 cells transfected with Cx43 alone or together with siRNA for Nedd4 were maintained in the presence or absence of serum. Lysates were subjected to extraction with 1% Triton X-100, and soluble and insoluble fractions were processed for immunoblot against the indicated proteins. (C) COS-7 cells transfected with wild-type Cx43 (Cx43WT) or the mCherry-Cx43-Ub plasmid alone or together with siRNA for Nedd4 were maintained in the presence or absence of serum and treated with 3MA where indicated and subjected to immunoblot for Cx43. (D) Immunofluorescence for Cx43 and β-catenin in NRK cells transfected with plasmids coding for wild-type (wt), ubiquitin tagged (-Ub), and endocytic mutant (Y286A) Cx43. Individual channels and merged images are shown. Bottom, insets at higher magnification. (E) Immunostaining for LC3 in NRK cells expressing wild-type GFP-Cx43 or ubiquitin-tagged mCherry-Cx43 maintained in the presence of serum. Merged channels are shown. (F) Immunostaining for p62 of COS-7 cells transiently expressing mCherry-Cx43-Ub and GFP-LC3 and maintained in the presence or absence of serum. Merged channels are shown. (G) Lysates of COS-7 cells transfected with Cx43 and maintained in the presence or absence of serum were subjected to extraction with 1% Triton X-100, and the soluble fraction was subjected to immunoprecipitation for Cx43 and immunoblotted for p62 and Cx43. Levels of p62 in the input are also shown. (H) Lysates from COS-7 cells transfected with Cx43 and/or mCherry-Cx43-Ub, maintained in the absence of serum and treated or not with 10 mM 3MA or 50 μM chloroquine (CQ), were immunoprecipitated with polyclonal antibodies directed against Cx43 and the precipitates immunoblotted for p62 or Cx43.

receptor substrate 15 (Eps15; Girao *et al.*, 2009). To directly analyze possible changes in ubiquitinylation of Cx43 upon macroautophagy activation, we first pulled down Cx43 in cells maintained in serum-supplemented or serum-deprived media to activate macroautophagy, and we immunoblotted for ubiquitin. As shown in Figure 6A, once normalized for the amount of Cx43 pulled down, we found a threefold increase in the level of ubiquitinylation of Cx upon serum removal (note that previous studies demonstrated that the ubiquitin laddering in Cx43 results from multiple monoubiquitinylation). These differences become more evident when lysosomal degradation was prevented (Figure 6A). Of interest, blockage of initiation of the autophagic process did not prevent the starvation-induced ubiquitinylation of Cx43, suggesting that this modification occurs before the sequestration in autophagosomes (Figure 6A).

Using similar procedures in cells expressing Cx43Y286A, we found that this mutant protein displayed compromised ubiquitinylation when compared with the wild-type protein, and starvation failed to induce an increase in the ubiquitinylation of this mutant protein (Supplemental Figure S6A). Besides the critical role of tyrosine 286 as part of the YXXØ internalization domain on Cx43, this residue is also part of the PY motif used for binding of the ubiquitin ligase Nedd4. We previously showed that Nedd4 mediates the ubiquitinylation of Cx43 required for the internalization and degradation of GJ by recruiting the endocytic protein Eps15 (Girao *et al.*, 2009). Consequently, to further evaluate the role of ubiquitin in macroautophagy of GJ, we knocked down Nedd4 and analyzed changes in Cx43 levels upon induction of macroautophagy. Depletion of Nedd4 resulted in almost complete blockage of the degradation of Cx43 induced by starvation, which mainly affects the population of Cx43 localized at GJs (Figure 6B).

To demonstrate that ubiquitinylation of Cx43 was directly responsible for inducing its macroautophagic degradation, we used cells expressing a mCherry-Cx43-Ub fusion protein, previously shown to incorporate in GJs and mediate their degradation even in the absence of Nedd4 (Catarino *et al.*, 2011). This form of Cx43 (Cx43-UbK48R) has a single molecule of ubiquitin that is mutated in its lysine 48 to prevent assembly of additional ubiquitin moieties and the formation of polyubiquitin chains. As observed for the wild-type protein, removal of serum increased the degradation of mCherry-Cx43-Ub, and it was possible to block this degradation by treatment with 3MA (Figure 6C). However, whereas knockdown of Nedd4 prevented the decrease in wild-type Cx43 observed after removal of serum in the control cells, part of mCherry-Cx43-Ub was still degraded when the Nedd4-deficient cells were deprived of serum (Figure 6C). The fact that this degradation of mCherry-Cx43-Ub was still sensitive to 3MA supports the idea that it took place by macroautophagy. Image analysis confirmed that in contrast to wild-type Cx43 and Cx43Y286A, which can be detected, for the most part, at the plasma membrane, Cx43-Ub localized in intracellular compartments (Figure 6D) that labeled positive for the autophagosomal marker LC3 (Figure 6E and Supplemental Figure S6D). Chemical (Supplemental Figure S6B) or genetic blockage of autophagy (Supplemental Figure S6C shows cells knocked down for Atg7) prevented mCherry-Cx43-Ub internalization and its association with autophagosomes. These results support the idea that fully functional macroautophagy is required for the rapid internalization and degradation of the constitutively ubiquitinylated form of Cx43.

Degradation of ubiquitinylated proteins by macroautophagy often requires participation of cargo-recognition molecules that bind both ubiquitin and LC3 to facilitate autophagosome formation around the cargo. The most common of these cargo recognition molecules is p62 (Pankiv *et al.*, 2007). We found that Cx43 colocalized

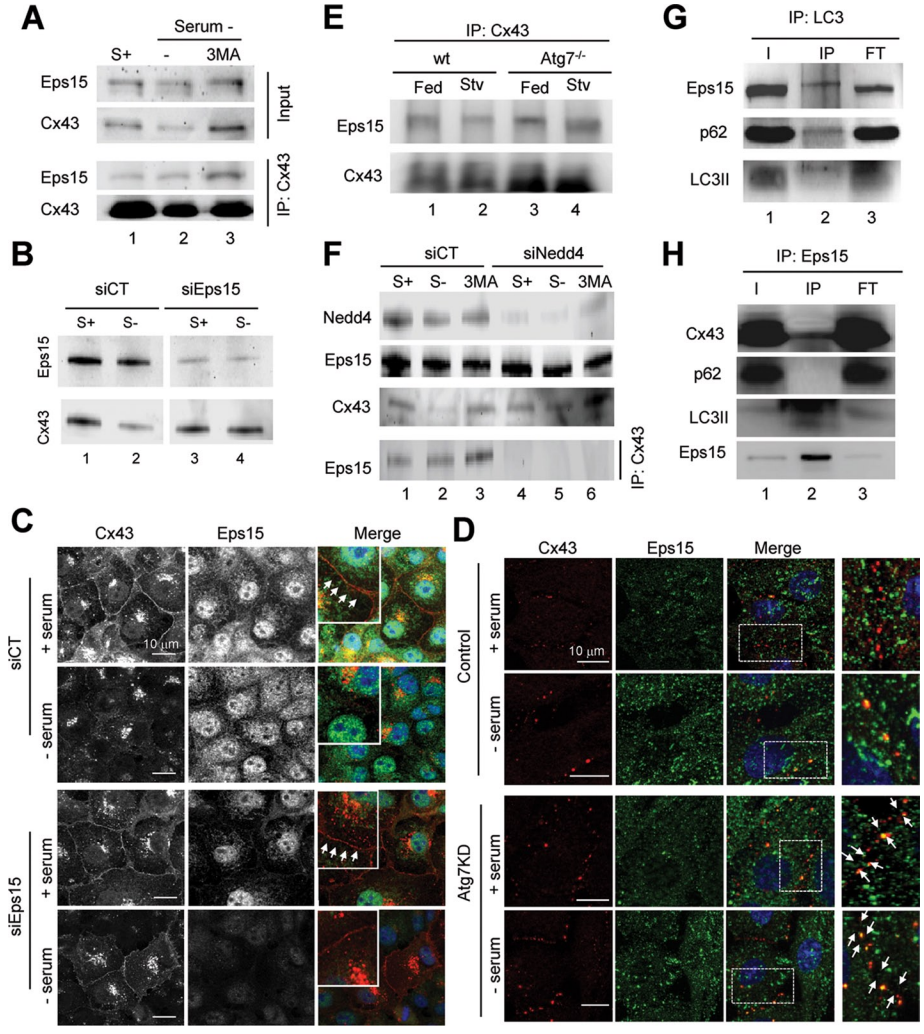

FIGURE 7: Degradation of GJ channels via macroautophagy requires binding of Eps15 to Cx. (A) COS-7 cells maintained in the presence (+) or absence (–) of serum and treated with 10 mM 3MA were subjected to immunoprecipitation for Cx43, followed by immunoblot for Cx43 and Eps15. Levels of Eps15 and Cx43 in the input fractions are also shown. (B) Immunoblot for Cx43 and Eps15 of COS-7 cells transfected with a control (CT) siRNA or siRNA for Eps15 and maintained in the presence or absence of serum as labeled. (C) Immunofluorescence for Cx43 (red) and Eps15 (green) in the same cells maintained in the presence or absence of serum as labeled. Single and merged channels are shown. Arrows point to the presence of Cx in the plasma membrane. (D) Immunofluorescence for Cx43 and Eps15 in NRK cells control or knockdown for Atg7 cells incubated in presence or absence of serum for 4 h. Right, higher-magnification images. (E) Immunoblot for Eps15 and Cx43 of immunoprecipitates for Cx43 in livers of wt or Alb-Cre-ATG7$^{f/f}$ (Atg7$^{-/-}$) mice. (F) Immunoblot for the indicated proteins in cells transfected with a control (CT) siRNA or siRNA for Nedd4 maintained in the presence or absence of serum and treated with 3MA as labeled. Bottom, levels of Eps15 in immunoprecipitates for Cx43 in the same cells. (G) Immunoblot for the indicated proteins in immunoprecipitates for LC3 in starved rat liver. (H) Immunoblot for the indicated proteins in immunoprecipitates for Eps15 in serum-deprived cells. Inputs (I), immunoprecipitates (IP), and flowthrough fraction (FT).

with p62 in the autophagosomal compartment (Figure 6F) and that, in fact, Cx43 interacts with p62. As shown in Figure 6G, p62 coimmunoprecipitated with Cx43, and starvation further increased the interaction between the two proteins. The amount of p62 that coimmunoprecipitated with Cx43 diminished in cells depleted of Nedd4, in further support of the hypothesis that ubiquitinylation of Cx43 is required to recruit p62. We further demonstrated by coimmunoprecipitation assays that degradation of the fusion protein Cx43-Ub also promotes its interaction with p62. As shown in Figure 6H, interaction between p62 and Cx43 significantly increased in cells expressing Cx43-Ub. Taken together, these data suggest that Nedd4-mediated ubiquitinylation of Cx43 is required to initiate the degradation of GJ Cx43 by macroautophagy.

Contribution of Eps15 to the early steps in macroautophagy of GJ connexin43

We analyzed the possible relationship between the previously described interaction of Cx43 with Eps15 and macroautophagy of GJ Cx43 (Girao *et al.*, 2009). We first assessed whether the interaction between Eps15 and Cx43 was altered during starvation. Cx43 immunoprecipitation in cells deprived of serum revealed a higher level of interacting Eps15 (relative to the amount of Cx43 pulled down) than in cells maintained in serum-supplemented media (Figure 7A). Enhanced interaction between Cx43 and Eps15 was even more apparent when macroautophagy of Cx43 was prevented by treatment with 3MA (Figure 7A). To determine whether the observed interaction with Eps15 was required for Cx43 degradation by macroautophagy, we knocked down Eps15. As shown in Figure 7B, we found that starvation-induced degradation of Cx43 was prevented in Eps15-deficient cells. Immunofluorescence analysis corroborated that in the absence of Eps15, most Cx43 remained at the plasma membrane even when serum was removed from the culture media (Figure 7C).

The formation of the Cx43/Eps15 complex was not disrupted if macroautophagy was prevented. In fact, in macroautophagy-compromised cells, the association of Eps15 with Cx at the plasma membrane was already very high under basal conditions and was not affected by the removal of serum (Figure 7D). Coimmunoprecipitation of Eps15 with Cx43 from livers of Atg7$^{-/-}$ mice (Figure 7E) or from MEFs from Atg5$^{-/-}$ mice (Supplemental Figure S7A) also confirmed higher interaction of both proteins in the autophagy-defective cells.

Then we explored whether the interaction of Cx43 with Eps15 in the early steps of the autophagic process was still dependent on the ubiquitinylation of Cx43. The previous pull-down studies for the endocytic mutant Cx43Y286A supported this hypothesis, as we confirmed that Eps15 no longer interacted with this mutant of Cx43, which also shows defective ubiquitinylation (Supplemental Figure S6A). Using cells knocked down for Nedd4, we found that Cx43 was no longer interacting with Eps15, not even when serum was removed or macroautophagy activation was prevented by treatment with 3MA (Figure 7F). These data support the idea that the association of Eps15 to Cx43 during macroautophagy is modulated by the ubiquitinylation state of Cx43

and that formation of this complex occurs prior to the recruitment of the macroautophagic machinery.

Last, we considered the possibility that Eps15 was acting as a novel autophagy cargo recognition molecule. A distinctive feature of this family of receptors is that they all interact simultaneously with LC3 and with cargo components (such as, e.g., ubiquitin moieties). Analysis of LC3 pull-downs revealed that a fraction of cellular Eps15 can be coimmunoprecipitated with this autophagosome marker, as is the case for p62 (Figure 7G and Supplemental Figure S7B). However, p62 and Eps15 do not seem to be part of the same complex with LC3, as in pull-down experiments with Eps15 we were able to retrieve LC3-II and Cx43 but not p62 (Figure 7H and Supplemental Figure S7B). These data support the idea that Eps15 acts as an intermediate bridge molecule between ubiquitinylated Cx43 and the autophagy machinery and opens up the possibility that Eps15 could be an autophagic adaptor for the degradation of GJ Cx43.

Overall our studies reveal a role for macroautophagy in the turnover of GJs that is interdependent with the internalization of Cxs from these regions of the plasma membrane. Ubiquitinylation of Cxs is necessary and sufficient to trigger the macroautophagy-dependent internalization of these constituents of the GJs and their subsequent turnover.

DISCUSSION

Degradation of structural components of GJs has been recognized as a regulatory mechanism for these structures (Musil *et al.*, 2000), and, in fact, in recent years strong evidence in support of the contribution of the ubiquitin–proteasome system, endolysosomes, and the autophagic system in this degradation has been presented (Laing *et al.*, 1997; Musil *et al.*, 2000; Qin *et al.*, 2003; Berthoud *et al.*, 2004; Leithe and Rivedal, 2004; Kelly *et al.*, 2007). In this work, we investigated the role of macroautophagy in the degradations of different Cxs and found that the autophagic system preferentially targets Cxs present at the plasma membrane and acts in fact as a modulator of the membrane content of Cxs under physiological conditions. This function becomes particularly relevant in response to nutritional stress, when a marked reduction in intercellular communication is normally observed.

Previous reports showed that Cx43 can undergo degradation in lysosomes by macroautophagy (Hesketh *et al.*, 2010; Lichtenstein *et al.*, 2011); however, the cellular pool of Cx43 targeted for macroautophagy and the molecular determinants that regulate this process were unknown. In this report, we show preferential macroautophagy of Cx43 present in GJs and demonstrate that targeting of GJ Cxs for macroautophagy is triggered by Nedd4-mediated ubiquitinylation of this protein. This modification recruits Eps15, a molecule that acts as an intermediate between Cxs and the autophagy machinery. Although most membrane proteins undergo degradation by endocytosis, as is also the case for a fraction of membrane Cxs, degradation of membrane proteins by macroautophagy is not without precedent, as several transmembrane proteins were reported to undergo degradation mediated by this autophagic pathway (Rowland *et al.*, 2006; Sanjuan *et al.*, 2007). In some of these cases the participation of only specific components of the autophagic machinery, such as LC3, rather than the whole autophagic process was described. However, we do not think that this is the case for Cx, because blockage of two different autophagy essential genes, Atg7 and Atg5, and chemical blockage of the kinase activity of Vps34 as part of the autophagy nucleation complex all had similar effect on Cx turnover and in its retention at the plasma membrane. Although the highest increase in Cxs upon macroautophagic blockage was observed at the plasma membrane, considering the marked reduction in total content of Cxs upon serum removal, we cannot eliminate the possibility that other sources of Cxs, such as secretory vesicles carrying Cxs toward the plasma membrane (VanSlyke *et al.*, 2000; Qin *et al.*, 2003), may also undergo degradation through macroautophagy.

An interesting aspect of our study, in light of the higher content of plasma membrane Cxs that we identified in cells with compromised macroautophagy even under basal conditions, is that macroautophagy may contribute to the continuous turnover of Cxs and thus to modulate intercellular connectivity under normal conditions. In fact, Cxs can even be detected in autophagosomes isolated from cells maintained under normal nutritional conditions. However, despite complete blockage of macroautophagy, some degradation still occurs, supporting the existence of overlapping mechanisms for Cx degradation. Some level of endocytic degradation of Cxs may still occur in most cells, and this pathway may be the one responsible for the small fraction of Cxs still degraded in cells with defective macroautophagy. The organization of Cxs at the plasma membrane (as monomers, hemichannels, or GJs) and the different posttranslational modifications that they undergo in this compartment might determine their degradation through one or another pathway.

Although transcripts for Cx43 can be detected in liver, overall levels of this Cx in hepatocytes are very low, as also confirmed by our immunochemistry analysis of wild-type mouse liver (Vinken *et al.*, 2008). In contrast, livers of Atg7-knockout mice display a dramatic increase in the content of Cx43. Considering the proposed function of Cx43 in controlling tissue volume (Rossello *et al.*, 2009), the high levels of expression of Cx43 in liver of Atg7-deficient mice could explain, in part, the hepatomegaly phenotype observed in these animals (Komatsu *et al.*, 2005). Although the increase in Cx43 in these animals could indirectly result as a response to the stress that cells with compromised macroautophagy undergo, the marked effect on Cx degradation observed in vitro makes it more likely that the high content of Cx43 in Atg7-deficient mice results from its compromised degradation. In this respect, it seems that most of Cx43 produced in hepatocytes is rapidly degraded, although the reasons for such an accelerated continuous turnover require further investigation.

The fact that Cx43 mutants that cannot be internalized are also resistant to degradation upon activation of macroautophagy (being retained at plasma membrane) supports the notion that internalization of Cx43 is, to a large extent, coupled to its degradation by macroautophagy. Data presented in this study are consistent with a model in which a cooperative mechanism involving both activation of macroautophagy and internalization participate in degradation of Cx43 at plasma membrane.

Phosphorylation and ubiquitinylation have been suggested to regulate the trafficking of Cxs from the plasma membrane to the lysosomes (Laing and Beyer, 1995; Berthoud *et al.*, 2004; Leithe *et al.*, 2009). We propose that part of this trafficking, initially attributed to classic endocytosis, instead takes place via macroautophagy. Ubiquitinylation is important for targeting of soluble cytosolic cargo to autophagosomes (Kirkin *et al.*, 2009), but this is the first report of its contribution to targeting of a membrane protein to this compartment. Our work supports the idea that ubiquitinylation of Cx43 appears to be an early event in this process and, according to our data, is required for the recruitment of the adaptor protein Eps15 facilitating interaction with the autophagy machinery. Of interest, proteins carrying Eps15-homology domains have been proposed to participate in macroautophagy in yeast and flies (Bugnicourt *et al.*, 2008; Csikos *et al.*, 2009). Although we cannot eliminate the possibility of some level of cooperation between Eps15 and the well-characterized

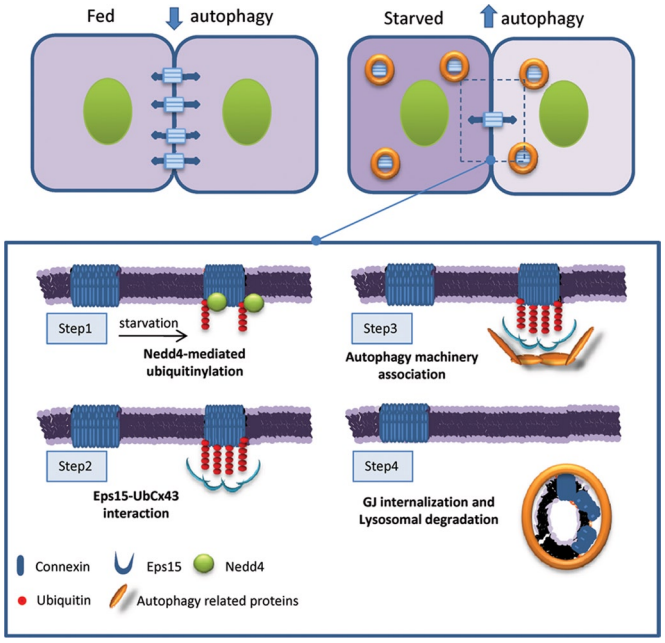

FIGURE 8: Degradation of GJ channels via macroautophagy requires Nedd4 mediated ubiquitinylation. GJ channels contribute to the metabolic and electrical coupling among adjacent cells. Starvation induces degradation of GJ connexins by macroautophagy and reduces intercellular communication. Macroautophagy of connexins is triggered by their ubiquitinylation by the ubiquitin ligase Nedd4 (step 1). Eps15 associates with the highly enriched ubiquitinylated GJ domains (step 2) and favors recruitment of the autophagic machinery (step 3), leading to connexin internalization and lysosomal degradation (step 4).

autophagic receptor p62, under our experimental conditions, they do not form part of the same Cx complex. The fact that we did not find p62 associated to the plasma membrane and that its colocalization with Cx43 mainly occurred in intracytoplasmic vesicles (Supplemental Figure S2B) supports that the observed interaction between p62 and Cx43 (Figure 6G) may be a postinternalization event. The presence of p62 in the Cx43-containing autophagosomes detected inside the cells could indicate the need for this receptor protein in the degradation of intracellular Cx43 by macroautophagy. Future studies are needed to determine whether p62 is solely required for degradation of de novo synthesized Cx43, as part of cellular quality control, or whether it also participates in the degradation of plasma membrane Cx43, but only once GJs have been internalized into the cytosolic compartment in a Eps15-dependent manner.

The canonical view for internalization of Cx43 involves formation of a large structure called an annular gap junction, which results from the internalization of both sides of the plaque by one of the two adjacent cells. It is possible thus that Eps15 may act as a preadaptor in the early stages of internalization of this annular structure, favoring docking of autophagy-related proteins. Conformational changes undergone by Cx43 later, after internalization, may be recognized by p62 and favor Cx43/p62 interaction. Although further studies are needed, we propose an additional level of complexity in the process of maturation of these structures of degradation emerging from the plasma membrane that involves a stepwise association of autophagic receptors (Figure 8).

The novel regulatory role for macroautophagy in cell interconnectivity proposed in this study may have physiological relevance under those conditions in which changes in the cell-to-cell interaction is required. Changes in macroautophagic activity in different pathologies or with age could thus alter cellular permeability and their ability to modulate cellular communication with the environment and neighboring cells. It is thus possible that altered autophagic activity underlies the basis of some of the severe Cx-associated pathologies, including cardiovascular disease, ocular diseases, diabetes, or cancer, as autophagic compromise has been described in all of these conditions (Mizushima *et al.*, 2008).

MATERIALS AND METHODS

Animals and cells

Adult male GFP-LC3, Alb-Cre-ATG7$^{f/f}$ (Komatsu *et al.*, 2005), and C57BL/6 mice were used in our study for subcellular fractionation under an animal study protocol approved by the Institutional Animal Care and Use Committee of the Albert Einstein College of Medicine. Where indicated, animals were starved for 6 h before organelle isolation by completely removing food but maintaining water supply ad libitum. NRK cells, COS-7 cells, and mouse fibroblasts (NIH3T3) from the American Type Culture Collection (Manassas, VA) and MEFs derived from wild-type and Atg5$^{-/-}$ mice (Kuma *et al.*, 2004) were maintained in DMEM (Sigma-Aldrich, St. Louis, MO) containing 10% fetal bovine serum, 50 μg/ml penicillin, and 50 μg/ml streptomycin at 37°C with 5% CO_2. When indicated, cells were washed three times with Hank's balanced salt solution (HBSS; Invitrogen, Carlsbad, CA) and placed in fresh medium without serum to activate the autophagic process. Lysosome-dependent degradation was inhibited by addition of 20 mM NH_4Cl and 100 μM leupeptin or 50 μM chloroquine and macroautophagy-dependent degradation by addition of 10 mM 3MA in the incubation media (Kaushik and Cuervo, 2009). Rapamycin 100 nM was added to stimulate macroautophagy and 50 mg/ml cycloheximide to stop protein synthesis.

Antibodies and chemicals

Materials were as described before (Singh *et al.*, 2009; Koga *et al.*, 2010; Martinez-Vicente *et al.*, 2010) or obtained from the following sources: antibodies against Cx43, β-catenin, and α-tubulin were from Sigma-Aldrich and against Cx43, Cx32, and Cx26 from Invitrogen; the antibody against BiP/GRP78, E-cadherin, and hsc70 (clone 13D3) were from BD Biosciences (San Diego, CA), against LAMP1 (clone 1D4B), from the Developmental Hybridoma Bank (University of Iowa, Iowa City, IA), against glyceraldehyde-3-phosphate dehydrogenase, Nedd4, Eps15, and actin from Abcam (Cambridge, MA), against LC3 from Cell Signaling Technology (Beverly, MA), and against cathepsin B and p62 from Santa Cruz Biotechnology (Santa Cruz, CA); the antibodies against Atg5 and Atg7 were from Novus Biologicals (Littleton, CO); and the monoclonal P4D1 antibody (which recognizes both polyubiquitin and monoubiquitin residues) was from Covance (Berkeley, CA) and the monoclonal FK1 antibody (which recognizes only K48 chains) was from Biomol International (Enzo Life Sciences, Plymouth, PA). All secondary antibodies for immunofluorescence were from Molecular Probes (Invitrogen). Formaldehyde and paraformaldehyde were from PerkinElmer Life and Analytical Sciences (Waltham, MA). Rapamycin, lindane, sulforhodamine B, and 3-methyladenine were from Sigma-Aldrich.

RNA interference and cell transfection

Cells were transfected with cDNA constructs encoding Dendra-Cx using Lipofectamine 2000 reagent (Invitrogen) according to manufacturer's instructions. The vector expressing GFP-LC3 was kindly provided by Tamotsu Yoshimori (Osaka University, Osaka, Japan). To generate the mCherry-Cx43-UbK48R(AA) construct, we subcloned Cx43-UbK48R(AA) cDNA into pcDNA ENTR BP mCherry C1 (Catarino *et al.*, 2011). Plasmids expressing GFP-Cx43 and RFP-Cx43 were

generated by cloning the appropriate cDNA into pENTR vectors containing either GFP or RFP.

Knockdown was performed by transfection with small interfering RNA (siRNA) against Nedd4 (s9416; GGAAGAUCCAAGAUUGAAAtt) or s9417 (GGCGAUUUGUAAACCGAAUtt), obtained from Ambion (Austin, TX; Silencer Select Pre-designed siRNA), or by cell transduction with lentivirus carrying short hairpin RNA construct against Atg7 (5′-GACTGCAGTGCAGATGA-3′ and 5′-AAGCACCATCATGCTGGATAT-3′), packed in 293T packing cells transfected by the calcium phosphate protocol. Supernatants containing viral particles were harvested after 72 h, and 1 ml of the supernatant was used for cell transduction after incubation in the presence of polybrene as described (Massey *et al.*, 2008).

Isolation of subcellular fractions from mouse liver

Autophagosomes (APGs), autophagolysosomes (APLs), and lysosomes were isolated from liver of fed or 6-h-fasted mice by centrifugation in a discontinuous metrizamide density gradient as described previously (Marzella *et al.*, 1982). Fractions were recovered from the different metrizamide interfaces (APG in 20–15%, APL in 20–24%, and lysosomes in the 26–24%) and washed by centrifugation in 0.25 M sucrose. Cytosolic fractions were prepared by centrifugation of the 17,000 × *g* supernatant at 100,000 × *g* for 1 h. The pellet of this centrifugation was used as the endoplasmic reticulum–enriched fraction.

Electrophoresis and immunoblot

Cell lysates were prepared by solubilization in RIPA buffer (1% Triton-X 100, 1% sodium deoxycholate, 0.1% SDS, 0.15 M NaCl, 0.01 M sodium phosphate, pH 7.2) containing protease inhibitors and phosphatase inhibitors. The solubilized fraction was recovered in the supernatant after centrifugation at 12,000 × *g* for 30 min, and protein concentration was determined by the Lowry method using bovine serum albumin (BSA) as a standard (Lowry *et al.*, 1951). Total cellular lysates were subjected to immunoblot according to conventional procedures (Towbin *et al.*, 1979). Briefly, samples were run on SDS–PAGE gels, transferred to polyvinylidene fluoride or nitrocellulose membranes, and, after blockage with low fat-milk, incubated with primary antibodies in 3% BSA. The proteins of interest were visualized by chemiluminescence using peroxidase-conjugated secondary antibodies in an LAS-3000 Imaging System (Fujifilm, Tokyo, Japan). Densitometric quantification was performed in unsaturated images using ImageJ (National Institutes of Health, Bethesda, MD). For samples run in different immunoblots a line containing the same sample was used in all of them and served for normalization of the densitometries of the different membranes. For bidimensional electrophoresis, isoelectric focusing was done using the Protean IEF Cell (Bio-Rad, Hercules, CA) at 20°C with rapid ramping to voltage 10,000 V at a current limit of 50 µA using ReadyStrip IPG Strips with a nonlinear 3–10 pH range (Bio-Rad).

Immunoprecipitation

Cells were rinsed with phosphate-buffered saline (PBS) at 4°C, resuspended in lysis buffer (190 mM NaCl, 50 mM Tris-HCl, 6 mM EDTA, 1% Triton X-100, pH 8.3) supplemented with a protease inhibitor cocktail (Roche, Indianapolis, IN), 2 mM phenylmethylsulfonyl fluoride (PMSF), and 10 mM iodoacetamide, and incubated on ice for 10 min. The samples were then centrifuged at 10,000 × *g* for 10 min and the supernatants used for immunoprecipitation. Briefly, protein A was incubated with polyclonal antibodies directed against Cx43. Nonspecific antibodies were used as controls. Incubations proceeded for 1 h at 4°C, followed by incubation with supernatants for 3 h at 4°C. The samples were then centrifuged, and the protein A–Sepharose sediments washed three times in an appropriate washing buffer (500 mM NaCl, 50 mM Tris-HCl, 6 mM EDTA, 1% Triton X-100, pH 8.3), resuspended in Laemmli buffer, and denatured at 100°C for 5 min.

Triton X-100 extraction

The detergent solubility assay with 1% Triton X-100 was performed as described previously (VanSlyke and Musil, 2000). Cells were resuspended in lysis buffer (190 mM NaCl, 50 mM Tris-HCl, 6 mM EDTA, 1% Triton X-100, pH 8.3) supplemented with protease inhibitor cocktail (Roche), 2 mM PMSF, and 10 mM iodoacetamide. Samples were then ultracentrifuged at 100,000 × *g* for 50 min and the supernatant recovered (Triton X-100–soluble fraction). The detergent-insoluble pellets were resuspended in lysis buffer supplemented with 0.1% SDS (Triton X-100–insoluble fraction) and sonicated. Laemmli buffer was then added to the Triton X-100–soluble and Triton X-100–insoluble fractions and denatured at 100°C for 5 min before SDS–PAGE and immunoblot analysis.

Biotinylation of cell surface proteins

COS-7 cells grown on 60-mm culture dishes were rinsed twice with 5 ml of ice-cold PBS containing 0.5 mM $MgCl_2$ and 1 mM $CaCl_2$, followed by the addition of 1.5 ml of the same ice-cold solution containing 1 mg/ml of freshly added Sulfo-NHS-SS-biotin (Pierce, Rockford, IL). After 30 min at 4°C, to stop subcellular trafficking, the medium was discarded and the plates were washed three times with PBS containing 0.5 mM $MgCl_2$, 1 mM $CaCl_2$, and 100 mM glycine. The cells were scraped in RIPA buffer (50 mM Tris-HCl, 150 mM NaCl, 5 mM ethylene glycol tetraacetic acid, containing 1% Triton X-100, 0.5% deoxycholate, and 0.1% SDS and supplemented with protease inhibitor cocktail [Roche], 2 mM PMSF, and 10 mM iodoacetamide, pH 7.5). After 15 min on ice the cells were sonicated, and the homogenates were centrifuged at 14,000 rpm for 10 min. Samples were then transferred to 1.5-ml Eppendorf microfuge tubes containing 100 µl of NeutrAvidin beads (Pierce). After 2 h of incubation at 4°C under agitation, the beads were washed four times with RIPA buffer. The final pellets were resuspended in 75 µl of 2× Laemmli buffer and denatured at 100°C for 5 min. The beads were pelleted, and the solubilized proteins were separated by SDS–PAGE, transferred to nitrocellulose membranes, and probed with antibodies directed against Cx43.

Immunofluorescence staining and image analysis

Indirect immunofluorescence was performed following conventional procedures. Cells were grown on coverslips, fixed for 10 min in either ice-cold methanol or 4% formaldehyde in PBS, blocked and permeabilized (1% BSA, 2% new-born calf serum, 0.01% Triton X-100), and then incubated with the primary and corresponding Alexa 488– or cyanine 5–conjugated secondary antibodies as described previously (Kaushik *et al.*, 2006). After immunostaining, cells were rinsed with PBS and mounted for microscopy using Fluoromount-G (SouthernBiotech, Birmingham, AL). Images were collected using either an Axiovert 200 fluorescence microscope (Carl Zeiss, Jena, Germany) equipped with a 63× objective and 1.4 numerical aperture and subjected to deconvolution with the manufacturer's software or a confocal microscope Leica SP5II AOBS (Leica, Wetzlar, Germany) equipped with 60× objective. In the case of isolated APGs, APLs, or lysosomes, vesicles were incubated for 10 min at room temperature with primary antibodies, followed by incubation with fluorescence-conjugated secondary antibodies for an additional 10 min as previously described (Koga *et al.*, 2010). Labeled

vesicles were recovered by centrifugation and spotted on a glass slide, fixed with 8% formaldehyde in 0.25 M sucrose for 15 min, and visualized with a 100× objective and 1.4 numerical aperture in the Axiovert 2000 fluorescence microscope. For quantitative analysis, number of fluorescent particles per cell was determined using the Analyze Particles function of ImageJ after applying a fixed threshold to all images. Percentage of colocalization was calculated using the JACoP plug-in in this software.

Electron microscopy and immunogold

Isolated organelles were pelleted, fixed in 4% paraformaldehyde/0.1% gluteraldehyde in 0.1 M sodium cacodylate, pH 7.43, dehydrated, and embedded in Lowicryl. Immunogold labeling was performed on ultrathin sections as described (Kaushik *et al.*, 2006). Briefly, each grid was washed in 50 mM glycine in phosphate-buffered saline, blocked, and incubated with the primary antibody and gold-conjugated secondary antibodies for 2 h each. After extensive washing, samples were fixed a second time for 5 min in 2% gluteraldehyde, washed, and negatively stained with 1% uranyl acetate for 15 min. Control grids were incubated with either an irrelevant immunoglobulin G and the secondary antibody under the same conditions or only with the secondary antibody. All grids were viewed on a JEOL 100CX II transmission electron microscope at 80 kV (JEOL, Peabody, MA).

Degradation analysis by image-based procedures

Degradation of Cxs in cultured cells was determined using the photoswitchable protein Dendra, which can be subjected to irreversible photoconversion from a green to a red fluorescent form. Cells expressing Dendra-Cx constructs for 2 4h were photoactivated by exposure to a 3.5-mA (current constant) light-emitting diode (405 nm; Norlux, Carol Stream, IL) for 10 min. At the desired times after photoconversion, cells were fixed in 4% paraformaldehyde, and images were captured with an Axiovert 200 fluorescence microscope. Quantification of total intensity was performed in individual frames using ImageJ in a minimum of 20 cells per condition. In other experiments, cells were harvested 8 h after photoconversion and analyzed by FACS to identify cells containing red and/or green fluorescence in 30,000 events. The decay of red fluorescence was used as an indicator of Cx degradation.

Gap junction permeability assay

Scrape-loading dye transfer technique was performed as described previously (Lai *et al.*, 2006). Briefly, cells were grown in six-well plates to confluence, washed three times with HBSS, and scratched with a sterile, broken razor blade. After incubation with (1.5 mg/ml) sulforhodamine B in HBSS for 3 min, cells were rinsed and fixed in 4% paraformaldehyde. Images were collected with an Axiovert 2000 fluorescence microscope with a 20× objective. A dye with red fluorescence emission was used for these studies because Atg7-knockdown cells coexpress GFP. To quantify dye transfer, the size of the fluorescence-occupied area was analyzed using Scion Image software in 40 fields per condition in at least three independent experiments.

Statistical analysis

All numerical results are reported as the mean ± SEM from a minimum of three independent experiments. GraphPad InStat software (GraphPad, La Jolla, CA) was used for analysis of statistical significance. For multiple comparisons a one-way analysis of variance followed by post hoc Tukey's test was used, and two-tailed Student's *t* test for unpaired data was used to evaluate single comparisons between different experimental groups. Differences were considered statistically significant for a value of $p < 0.05$ (denoted by an asterisk).

ACKNOWLEDGMENTS

We acknowledge Masaaki Komatsu for the ATG7$^{f/f}$ mice. We are grateful to Susmita Kaushik and Samantha J. Orenstein for their critical review of this work and Francisco Lazaro for his technical assistance with several of the image-based procedures. This work was supported in part by National Institutes of Health Grants DK041918 (to A.M.C. and D.S.), AG021904, and AG19834 (to A.M.C.) and by Foundation for Science and Technology Grant PTDC/SAU-ORG/113542/2009 (to P.P.).

REFERENCES

Berthoud VM, Minogue PJ, Guo J, Williamson EK, Xu X, Ebihara L, Beyer EC (2003). Loss of function and impaired degradation of a cataract-associated mutant connexin50. Eur J Cell Biol 82, 209–221.

Berthoud VM, Minogue PJ, Laing JG, Beyer EC (2004). Pathways for degradation of connexins and gap junctions. Cardiovasc Res 62, 256–267.

Bugnicourt A, Mari M, Reggiori F, Haguenauer-Tsapis R, Galan JM (2008). Irs4p and Tax4p: two redundant EH domain proteins involved in autophagy. Traffic 9, 755–769.

Catarino S, Ramalho JS, Marques C, Pereira P, Girao H (2011). Ubiquitin-mediated internalization of connexin43 is independent of the canonical endocytic tyrosine-sorting signal. Biochem J 437, 255–267.

Csikos G, Lippai M, Lukacsovich T, Juhasz G, Henn L, Erdelyi M, Maroy P, Sass M (2009). A novel role for the *Drosophila* epsin (lqf): involvement in autophagy. Autophagy 5, 636–648.

Defamie N, Mograbi B, Roger C, Cronier L, Malassine A, Brucker-Davis F, Fenichel P, Segretain D, Pointis G (2001). Disruption of gap junctional intercellular communication by lindane is associated with aberrant localization of connexin43 and zonula occludens-1 in 42GPA9 Sertoli cells. Carcinogenesis 22, 1537–1542.

el-Fouly MH, Trosko JE, Chang CC (1987). Scrape-loading and dye transfer. A rapid and simple technique to study gap junctional intercellular communication. Exp Cell Res 168, 422–430.

Ginzberg RD, Gilula NB (1979). Modulation of cell junctions during differentiation of the chicken otocyst sensory epithelium. Dev Biol 68, 110–129.

Girao H, Catarino S, Pereira P (2009). Eps15 interacts with ubiquitinated Cx43 and mediates its internalization. Exp Cell Res 315, 3587–3597.

Govindarajan R, Chakraborty S, Johnson KE, Falk MM, Wheelock MJ, Johnson KR, Mehta PP (2010). Assembly of connexin43 into gap junctions is regulated differentially by E-cadherin and N-cadherin in rat liver epithelial cells. Mol Biol Cell 21, 4089–4107.

Guan X, Ruch RJ (1996). Gap junction endocytosis and lysosomal degradation of connexin43-P2 in WB-F344 rat liver epithelial cells treated with DDT and lindane. Carcinogenesis 17, 1791–1798.

Hesketh GG, Shah MH, Halperin VL, Cooke CA, Akar FG, Yen TE, Kass DA, Machamer CE, Van Eyk JE, Tomaselli GF (2010). Ultrastructure and regulation of lateralized connexin43 in the failing heart. Circ Res 106, 1153–1163.

Kabeya Y, Mizushima N, Ueno T, Yamamoto A, Kirisako T, Noda T, Kominami E, Ohsumi Y, Yoshimori T (2000). LC3, a mammalian homologue of yeast Apg8p, is localized in autophagosome membranes after processing. EMBO J 19, 5720–5728.

Kaushik S, Cuervo AM (2009). Methods to monitor chaperone-mediated autophagy. Methods Enzymol 452, 297–324.

Kaushik S, Massey AC, Cuervo AM (2006). Lysosome membrane lipid microdomains: novel regulators of chaperone-mediated autophagy. EMBO J 25, 3921–3933.

Kelly SM, Vanslyke JK, Musil LS (2007). Regulation of ubiquitin-proteasome system mediated degradation by cytosolic stress. Mol Biol Cell 18, 4279–4291.

Kirkin V, McEwan DG, Novak I, Dikic I (2009). A role for ubiquitin in selective autophagy. Mol Cell 34, 259–269.

Koga H, Kaushik S, Cuervo AM (2010). Inhibitory effect of intracellular lipid load on macroautophagy. Autophagy 6, 825–827.

Komatsu M *et al.* (2005). Impairment of starvation-induced and constitutive autophagy in Atg7-deficient mice. J Cell Biol 169, 425–434.

Kuma A, Hatano M, Matsui M, Yamamoto A, Nakaya H, Yoshimori T, Ohsumi Y, Tokuhisa T, Mizushima N (2004). The role of autophagy during the early neonatal starvation period. Nature 432, 1032–1036.

Kumar NM, Gilula NB (1996). The gap junction communication channel. Cell 84, 381–388.
Lai A, Le DN, Paznekas WA, Gifford WD, Jabs EW, Charles AC (2006). Oculodentodigital dysplasia connexin43 mutations result in non-functional connexin hemichannels and gap junctions in C6 glioma cells. J Cell Sci 119, 532–541.
Laing JG, Beyer EC (1995). The gap junction protein connexin43 is degraded via the ubiquitin proteasome pathway. J Biol Chem 270, 26399–26403.
Laing JG, Tadros PN, Westphale EM, Beyer EC (1997). Degradation of connexin43 gap junctions involves both the proteasome and the lysosome. Exp Cell Res 236, 482–492.
Leithe E, Kjenseth A, Sirnes S, Stenmark H, Brech A, Rivedal E (2009). Ubiquitylation of the gap junction protein connexin-43 signals its trafficking from early endosomes to lysosomes in a process mediated by Hrs and Tsg101. J Cell Sci 122, 3883–3893.
Leithe E, Rivedal E (2004). Epidermal growth factor regulates ubiquitination, internalization and proteasome-dependent degradation of connexin43. J Cell Sci 117, 1211–1220.
Lichtenstein A, Minogue PJ, Beyer EC, Berthoud VM (2011). Autophagy: a pathway that contributes to connexin degradation. J Cell Sci 124, 910–920.
Lowry OH, Rosebrough NJ, Farr AL, Randall RJ (1951). Protein measurement with the Folin phenol reagent. J Biol Chem 193, 265–275.
Martinez-Vicente M *et al*. (2010). Cargo recognition failure is responsible for inefficient autophagy in Huntington's disease. Nat Neurosci 13, 567–U574.
Marzella L, Ahlberg J, Glaumann H (1982). Isolation of autophagic vacuoles from rat liver: morphological and biochemical characterization. J Cell Biol 93, 144–154.
Massey AC, Follenzi A, Kiffin R, Zhang C, Cuervo AM (2008). Early cellular changes after blockage of chaperone-mediated autophagy. Autophagy 4, 442–456.
Mizushima N, Levine B, Cuervo AM, Klionsky DJ (2008). Autophagy fights disease through cellular self-digestion. Nature 451, 1069–1075.
Musil LS, Le AC, VanSlyke JK, Roberts LM (2000). Regulation of connexin degradation as a mechanism to increase gap junction assembly and function. J Biol Chem 275, 25207–25215.
Pankiv S, Clausen TH, Lamark T, Brech A, Bruun JA, Outzen H, Overvatn A, Bjorkoy G, Johansen T (2007). p62/SQSTM1 binds directly to Atg8/LC3 to facilitate degradation of ubiquitinated protein aggregates by autophagy. J Biol Chem 282, 24131–24145.
Pfeifer U (1980). Autophagic sequestration of internalized gap junctions in rat liver. Eur J Cell Biol 21, 244–246.
Qin H, Shao Q, Igdoura SA, Alaoui-Jamali MA, Laird DW (2003). Lysosomal and proteasomal degradation play distinct roles in the life cycle of Cx43 in gap junctional intercellular communication-deficient and -competent breast tumor cells. J Biol Chem 278, 30005–30014.
Rossello RA, Wang Z, Kizana E, Krebsbach PH, Kohn DH (2009). Connexin 43 as a signaling platform for increasing the volume and spatial distribution of regenerated tissue. Proc Natl Acad Sci USA 106, 13219–13224.
Rowland AM, Richmond JE, Olsen JG, Hall DH, Bamber BA (2006). Presynaptic terminals independently regulate synaptic clustering and autophagy of GABAA receptors in *Caenorhabditis elegans*. J Neurosci 26, 1711–1720.
Sanjuan MA *et al*. (2007). Toll-like receptor signalling in macrophages links the autophagy pathway to phagocytosis. Nature 450, 1253–1257.
Seglen PO, Gordon PB (1982). 3-Methyladenine: specific inhibitor of autophagic/lysosomal protein degradation in isolated rat hepatocytes. Proc Natl Acad Sci USA 79, 1889–1892.
Singh R, Xiang Y, Wang Y, Baikati K, Cuervo AM, Luu YK, Tang Y, Pessin JE, Schwartz GJ, Czaja MJ (2009). Autophagy regulates adipose mass and differentiation in mice. J Clin Invest 119, 3329–3339.
Thomas MA, Zosso N, Scerri I, Demaurex N, Chanson M, Staub O (2003). A tyrosine-based sorting signal is involved in connexin43 stability and gap junction turnover. J Cell Sci 116, 2213–2222.
Towbin H, Staehelin T, Gordon J (1979). Electrophoretic transfer of proteins from polyacrylamide to nitrocellulose sheets: procedure and some applications. Proc Natl Acad Sci 76, 4350–4354.
VanSlyke JK, Deschenes SM, Musil LS (2000). Intracellular transport, assembly, and degradation of wild-type and disease-linked mutant gap junction proteins. Mol Biol Cell 11, 1933–1946.
VanSlyke JK, Musil LS (2000). Analysis of connexin intracellular transport and assembly. Methods 20, 156–164.
Vinken M, Henkens T, De Rop E, Fraczek J, Vanhaecke T, Rogiers V (2008). Biology and pathobiology of gap junctional channels in hepatocytes. Hepatology 47, 1077–1088.